POLITECNICO DI TORINO
Repository ISTITUZIONALE

Geodesy and metrology with a transportable optical clock

Original
Geodesy and metrology with a transportable optical clock / Grotti, J., Koller, S., Vogt, S., Häfner, S., Sterr, U., Lisdat, C., Denker, H., Voigt, C., Timmen, L., Rolland, A., Baynes, F.N., Margolis, H.S., Zampaolo, M., Thoumany, P., Pizzocaro, M., Rauf, B., Bregolin, F., Tampellini, A., Barbieri, P., Zucco, M., et al.. - In: NATURE PHYSICS. - ISSN 1745-2473. - ELETTRONICO. - (2018). [10.1038/s41567-017-0042-3]

Availability:
This version is available at: 11583/2699696 since: 2018-02-13T14:38:09Z

Publisher:
Springer Nature

Published
DOI:10.1038/s41567-017-0042-3

Terms of use:

This article is made available under terms and conditions as specified in the corresponding bibliographic description in the repository

Publisher copyright

(Article begins on next page)

07 November 2026

nature physics

LETTERS

https://doi.org/10.1038/s41567-017-0042-3

Geodesy and metrology with a transportable optical clock

Jacopo Grotti[1], Silvio Koller[1], Stefan Vogt[1], Sebastian Häfner[1], Uwe Sterr[1], Christian Lisdat[1*], Heiner Denker[2], Christian Voigt[2,3], Ludger Timmen[2], Antoine Rolland[4], Fred N. Baynes[4], Helen S. Margolis[4], Michel Zampaolo[5], Pierre Thoumany[6], Marco Pizzocaro[6], Benjamin Rauf[6,7], Filippo Bregolin[6,7], Anna Tampellini[6,7], Piero Barbieri[6,7], Massimo Zucco[6], Giovanni A. Costanzo[6,7], Cecilia Clivati[6], Filippo Levi[6] and Davide Calonico[6]

Optical atomic clocks, due to their unprecedented stability[1–3] and uncertainty[3–6], are already being used to test physical theories[7,8] and herald a revision of the International System of Units[9,10]. However, to unlock their potential for cross-disciplinary applications such as relativistic geodesy[11], a major challenge remains: their transformation from highly specialized instruments restricted to national metrology laboratories into flexible devices deployable in different locations[12–14]. Here, we report the first field measurement campaign with a transportable ^{87}Sr optical lattice clock[12]. We use it to determine the gravity potential difference between the middle of a mountain and a location 90 km away, exploiting both local and remote clock comparisons to eliminate potential clock errors. A local comparison with a ^{171}Yb lattice clock[15] also serves as an important check on the international consistency of independently developed optical clocks. This campaign demonstrates the exciting prospects for transportable optical clocks.

The application of clocks in geodesy fulfils long-standing proposals to interpret a measurement of the relativistic redshift $\Delta\nu_{rel}$ between clocks at two sites as the associated gravity potential difference $\Delta U = c^2\,\Delta\nu_{rel}/\nu_0$ (ν_0 being the clock's frequency and c the speed of light)[11]. National geodetic height systems based on classical terrestrial and satellite-based measurements exhibit discrepancies at the decimetre level[16]. Optical clocks, combined with high-performance frequency dissemination techniques[17,18], offer an attractive way to resolve these discrepancies, as they combine the advantage of high spectral resolution with small error accumulation over long distances[17,19].

A clock-based approach to geodesy with a capability competitive with current techniques requires high clock performance: a fractional frequency accuracy of 1×10^{-17} corresponds to a resolution of about 10 cm in height. Furthermore, it is important to realize that the side-by-side frequency ratio has to be known to determine the remote frequency shift $\Delta\nu_{rel}$. Taking the uncertainty budgets of optical clocks for granted harbours the possibility of errors, because very few have been verified experimentally to the low 10^{-17} region or beyond[4,6,17,20]. A transportable optical clock not only increases the flexibility in measurement sites but mitigates the risk of undetected errors by enabling local calibrations to be performed.

The test site chosen for our demonstration of chronometric levelling[11] with optical clocks was the Laboratoire Souterrain de Modane (LSM) in France, with the Italian metrology institute INRIM in Torino serving as the reference site. The height difference between the two sites is approximately 1,000 m, corresponding to a fractional redshift of about 10^{-13}. From a geodetic point of view, LSM is an interesting location at which to make such measurements: first it is located in the middle of the 13 km long Fréjus road tunnel (rock coverage 1,700 m), and second the area exhibits long-term land uplift (Alpine orogeny) accompanied by a secular gravity potential variation. Furthermore, LSM lacks the metrological infrastructure to independently validate components of the clock and the environmental control on which the operation of optical clocks usually relies. The air temperature is high (~26 °C), with fluctuations of several Kelvin at the transportable clock, and the humidity is very low. Working hours are also severely restricted for safety reasons, a problem that was further compounded during our measurement campaign by interruptions due to blasts caused by construction of a new tunnel nearby. Even without this additional source of seismic noise, the acoustic noise levels in the laboratory are high. The selected location thus constitutes a challenging but realistic testbed with practical relevance.

The transportable ^{87}Sr lattice clock is (compared with laboratory clocks) designed to be compact, with robust optical parts[12]. The physics package is less than 0.6 m^3 in size, and we use laser breadboards with mechanical stress-resistant fibre couplers[21]. All components except the reference cavity of the interrogation laser are rigidly mounted in a car trailer (size 2.2 m × 3 m × 2.2 m), and vibration isolation is provided by rubber dampers. The trailer interior is temperature stabilized, while the small volume of the trailer hinders air exchange and generates hot spots with more than 10 K temperature rise. However, the optics and the physics package are placed apart and shielded from these and are stable to within 0.4 K after an initial temperature rise of about 1 K. The transportable ultrastable reference cavity for the clock interrogation lasers is rigidly mounted to endure transport[12]. It was placed next to the trailer to avoid its performance being degraded by vibrations induced in the trailer's air conditioning system. The vibration amplitudes in the trailer are a factor of ten larger than under typical laboratory conditions, leading to a corresponding increase in clock instability. A reference resonator with lower acceleration sensitivity or an active feed-forward system may in the future remedy this inconvenience[22].

[1]Physikalisch-Technische Bundesanstalt, Braunschweig, Germany. [2]Institut für Erdmessung, Leibniz Universität Hannover, Hannover, Germany. [3]GFZ German Research Centre for Geosciences, Potsdam, Germany. [4]National Physical Laboratory, Teddington, Middlesex, UK. [5]Laboratoire Souterrain de Modane, Carré Sciences, Modane, France. [6]Istituto Nazionale di Ricerca Metrologica (INRIM), Physical Metrology Division, Torino, Italy. [7]Dipartimento di Elettronica e Telecomunicazioni, Politecnico di Torino, Torino, Italy. *e-mail: christian.lisdat@ptb.de

© 2018 Macmillan Publishers Limited, part of Springer Nature. All rights reserved.

The Sr clock was operated in both locations, LSM and INRIM, to eliminate the need for a priori knowledge of the clock's frequency. A schematic outline of the experiment is given in Fig. 1. LSM and INRIM were connected by a 150 km noise-compensated optical fibre link (see Methods). At LSM, a transportable frequency comb measured the optical frequency ratio between a laser resonant with the Sr clock transition at 698 nm and 1.542 μm radiation from an ultrastable link laser transmitted from INRIM. In this way, the frequency of the optical clock at LSM could be directly related to the frequency of the link laser even without a highly accurate absolute frequency reference. In addition to the optical carrier, the fibre link was used to disseminate a 100 MHz radiofrequency reference signal from INRIM for the frequency comb, frequency counters and acousto-optic modulators at LSM (see Methods). At INRIM, a cryogenic Cs fountain clock[23] and a ^{171}Yb optical lattice clock[15] served as references. The connection between the clocks at INRIM and the link laser is provided by a second frequency comb.

Ten days after arriving at LSM in early February 2016, the first spectra of motional sidebands on the $^1S_0$–$^3P_0$ clock transition were recorded from the ^{87}Sr transportable clock, marking the point at which a recharacterization of the clock could begin. This set-up time included general logistics, powering and thermalization of the equipment, installation of reference frequency equipment, realignment of optical fibre couplings, individual testing of all subcomponents and magnetic field compensation for loading the atoms into the lattice. The operation of the lattice clock (see Methods) was similar to the procedure described in previous works[12].

The transportable clock operated less reliably in the environmental conditions at LSM than in initial tests at PTB before transport. Vibrations caused by the tunnel blasting mentioned earlier led to degradation of the light delivery for the first cooling stage of the magneto-optical trap (MOT; see Methods), which in turn led to interruptions due to insufficient atom number. The low-humidity environment also hampered the air conditioning in the trailer, causing the Ti:sapphire laser used to create the optical lattice to overheat, further shortening the clock operation periods and thus the evaluation of some contributions to the clock uncertainty budget. The blackbody radiation (BBR) shift was still controlled to the level of 3×10^{-17}. For these reasons, during the allocated time in the tunnel simultaneous operation was achieved only with the primary Cs fountain clock at INRIM and not with the high-stability Yb lattice clock. Although the Yb lattice clock at INRIM operated reliably for the majority of the time, the commercial lattice laser for the clock failed just before the characterization of the transportable clock had been completed. With the transportable clock operating for 2.8 h over two days at the end of the LSM campaign in mid-March 2016, the instability of the fountain clock ($2.2\times10^{-13}\,\tau^{-1/2}$, where τ is given in seconds) poses a limitation on the uncertainty of the frequency measurement. We therefore apply a hydrogen maser as a flywheel[24] to reduce the statistical uncertainty of the measurement: the maser's frequency is rapidly and accurately calibrated by the optical clock, and due to the frequency stability of the maser this calibration is valid for longer periods of time. This makes it possible to extend the averaging time to 48 h (see Methods), leading to an uncertainty of 17×10^{-16} associated with the measurement time. With systematic uncertainties of the Sr and Cs clocks of 2.6×10^{-16} and 3×10^{-16} respectively (see Table 1, Methods and ref. [23]), the frequency of the Sr lattice clock at LSM was measured by the fountain clock at INRIM with an uncertainty of 18×10^{-16} (see Fig. 1).

As noted earlier, an initial frequency comparison at a common gravity potential is required to transform a general frequency measurement or clock comparison into a chronometric levelling measurement. For this reason, the Sr apparatus was moved to INRIM in April 2016 for local clock comparisons. There, it was directly linked to the INRIM frequency comb. In the process, small upgrades were made to the set-up for the cooling light distribution and the

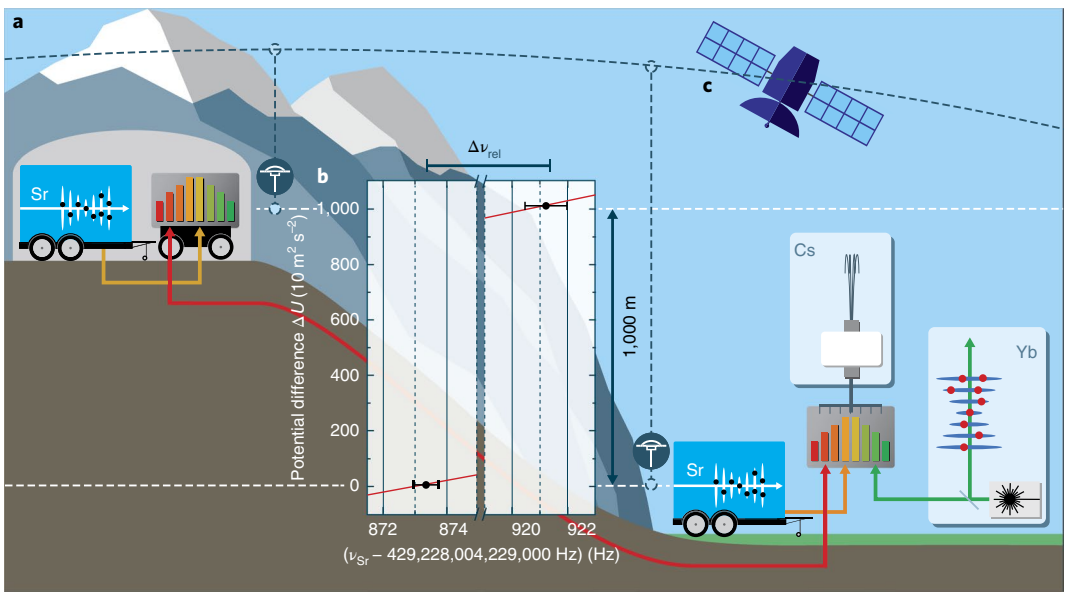

Fig. 1 | Schematic representation of the measurement campaign. a, For chronometric levelling, the transportable ^{87}Sr optical lattice clock was placed in the LSM underground laboratory close to the France–Italy border in the Fréjus tunnel (top left). The clock was connected by a noise-compensated fibre link (length 150 km) to the Italian national metrology institute INRIM in Torino (red line). There, a primary Cs fountain clock and a ^{171}Yb optical lattice clock were operated (right). At both sites, frequency combs were used to relate the frequencies of the $^1S_0$–$^3P_0$ optical clock transitions and the 1.5 μm laser radiation transmitted through the link. After the remote frequency comparison, the transportable clock was moved to INRIM for a side-by-side frequency ratio measurement. **b**, Frequency of the transportable Sr clock as seen by the INRIM Cs fountain clock (black circles, uncertainties are one standard deviation of the combined uncertainties). The potential difference ΔU is based on the geodetic measurement. The red line shows the expected variation of the Sr clock transition frequency due to the relativistic redshift. **c**, The potential difference between LSM and INRIM was also determined independently by a combination of GNSS (global navigation satellite system), spirit levelling and gravimetric geoid modelling (see Methods).

© 2018 Macmillan Publishers Limited, part of Springer Nature. All rights reserved.

Table 1 | Typical uncertainty budgets of the optical clocks

	^{171}Yb clock		^{87}Sr clock at LSM		^{87}Sr clock at INRIM	
	Correction	Uncertainty	Correction	Uncertainty	Correction	Uncertainty
Systematic effect	**($\times10^{-17}$)**		**($\times10^{-17}$)**		**($\times10^{-17}$)**	
Linear lattice light shift	4	8	0	24	0	17
Higher-order lattice shifts	12	10	−1.0	0.7	−0.5	0.7
Density shift	2	6	−1.2	3.0	−2.2	5.3
2nd-order Zeeman shift	27	4	34.2	0.5	11.7	0.2
BBR	237.4	2.6	500.3	3.4	515.3	1.8
Probe light shift	−1.0	3.5	0.2	0.2	0.3	0.3
D.c. Stark shift	0	1	0	0.1	0	0.1
Servo error	0	1	0	9.4	0	3.7
Line pulling	0	0.4	0	4.1	0	1.1
Optical path length	0	5	0	0.8	0	1.3
Acousto-optic modulator switching	0	0.4	—	—	—	—
Total	**281**	**16**	**532**	**27**	**524**	**18**

For the Sr lattice clock, we give the uncertainties for the measurements at LSM (first column) and INRIM (second column). All uncertainties correspond to one standard deviation.

thermal management in the car trailer. With these changes, the availability of the Sr clock was improved significantly, allowing for several hours of data taking per day after the initial set-up phase was completed. With systematic uncertainties comparable to the first campaign and a fountain instability of $3.6\times10^{-13}\,\tau^{-1/2}$, the total uncertainty was reduced by a factor of two to 9×10^{-16} (see Methods for Sr transition frequencies). In this chronometric levelling demonstration, we resolved a relativistic redshift of the optical lattice clock of 47.92(83) Hz (Fig. 1), from which we infer a potential difference of 10,034(174) m^2 s^{-2} (The numbers in the parentheses are the 1σ uncertainties referred to the corresponding last digits of the quoted results.). This is in excellent agreement with the value of 10,032.1(16) m^2 s^{-2} determined independently by geodetic means (see Methods). Though our result does not yet challenge the classical geodetic approach in accuracy, it is the first demonstration of chronometric levelling using a transportable optical clock.

With the increased reliability of the transportable Sr clock, we were also able to measure its optical frequency ratio R with the Yb lattice clock[15] operated on the $^1S_0$–$^3P_0$ transition at 578 nm. In total, 31,000 s of common operation of the two optical clocks and the frequency comb were achieved over a period of 7 days. This optical–optical comparison (Fig. 2) shows much higher stability than the optical–microwave one. Consequently, the optical frequency ratio measurement is limited by the systematic uncertainty of the clocks (Table 1), rather than by their instability. This demonstrates the key advantage of optical frequency standards: they are able to achieve excellent uncertainties in short averaging times even though they may operate less reliably than their microwave counterparts.

The ^{171}Yb/^{87}Sr frequency ratios measured on different days are summarized in Fig. 3, which also shows previous measurements of this ratio. After averaging (see Methods), we determine the ratio to be $R=\nu_{Yb}/\nu_{Sr}=1.207,507,039,343,338,41(34)$. Independent measurements of particular optical frequency ratios are important to check the consistency of optical clocks worldwide[25], and are key to establishing more accurate representations of the second[26] as provided by the International Committee for Weights and Measures (CIPM) as a step towards a future redefinition of the second. To our knowledge, this is the only optical frequency ratio that has been measured directly by three independent research groups[27–29]; however, our measurement differs from the most accurate previous measurement by two standard deviations (Fig. 3), and the origin of this difference will require further investigation by the research groups concerned.

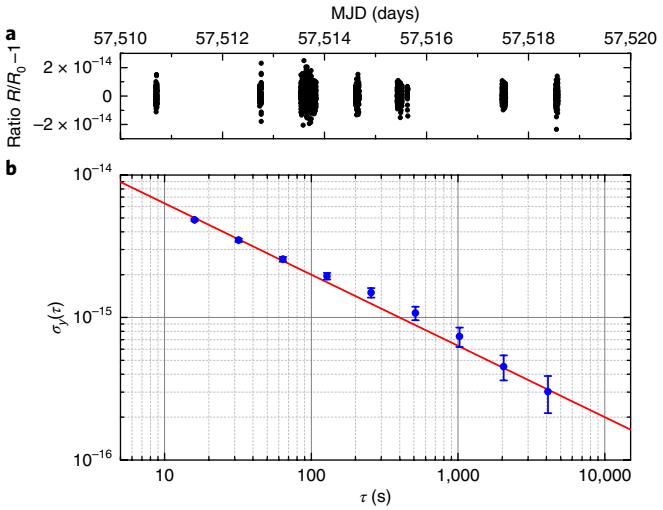

Fig. 2 | Instability of the measured fractional Yb/Sr frequency ratio R/R_0. a, Fractional optical frequency ratio R/R_0, averaged over 16 s intervals, as a function of the modified Julian date MJD. Here, $R_0=1.207,507,039,343,338,122$ as derived from the CIPM recommended frequencies for the ^{171}Yb and ^{87}Sr lattice clocks[26]. **b**, Fractional instability of R/R_0 (circles) derived from the concatenated data set in **a** and expressed as the Allan deviation σ_y. Error bars denote one standard deviation. The red line depicts an instability of $2\times10^{-14}\,\tau^{-1/2}$. The instability of R/R_0 arises from the instabilities of the two clocks involved in the comparison as well as the measurement chain. The stability of each individual clock depends on its clock laser, and separating their contributions is not straightforward. The instability of the Sr clock is estimated to be about $7\times10^{-15}\,\tau^{-1/2}$ from the instability of the frequency offset between the Sr clock transition and the clock laser reference cavity, after removing a linear cavity drift. The contribution from the Yb clock is probably more than $1\times10^{-14}\,\tau^{-1/2}$.

© 2018 Macmillan Publishers Limited, part of Springer Nature. All rights reserved.

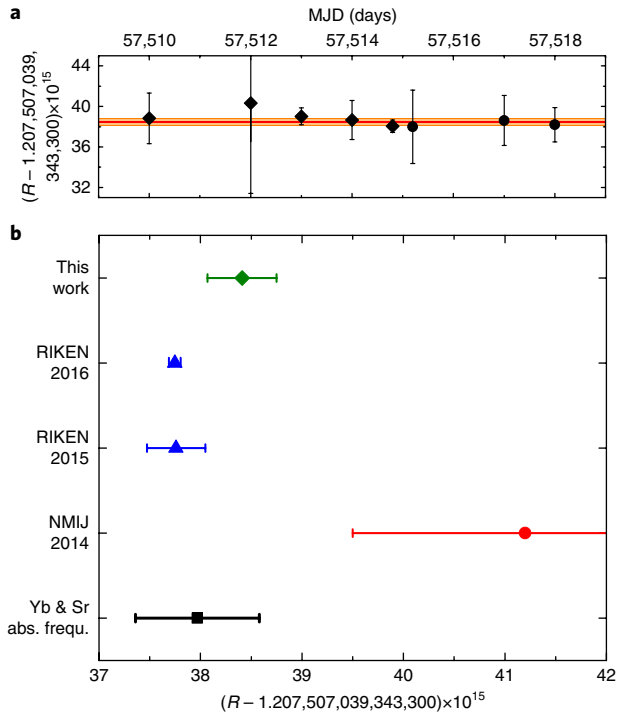

Fig. 3 | Comparison of frequency ratios *R* between ^{171}Yb and ^{87}Sr lattice clocks. a, Averages of the ratios measured on different days (diamonds and circles) and their overall average (line) with its respective uncertainty (coloured bar). Diamonds (circles) denote the operation of the Sr lattice clock with a shallow (deep) lattice (see Methods). **b**, Optical frequency ratios between ^{171}Yb and ^{87}Sr have been measured directly in only three groups so far (RIKEN 2016[27] and 2015[28], NMIJ 2014[29] and this work). The lowest point shows the ratio as inferred from averaging all published absolute frequency measurements for ^{171}Yb and ^{87}Sr (see Methods). All error bars represent one standard deviation of the total measurement uncertainty.

Note that, even with the only slightly improved transportable Sr apparatus as used at INRIM, chronometric levelling against the Yb lattice clock with considerably improved resolution would be possible. We expect that the transportable clock with improved reliability will be able to achieve an uncertainty of 1×10^{-17} before, for example, BBR-related uncertainties pose a limitation to the present set-up. Instabilities of $1\times10^{-15}\ \tau^{-1/2}$ are realistic with the current interrogation laser; lower instabilities will require an improved reference cavity. The uncertainty will enable height differences of 10 cm to be resolved, which is a relevant magnitude for geodesy in regions such as islands, which are hard to access using conventional geodetic approaches. As metrological fibre links become more common, chronometric levelling along their paths[30] will become a realistic prospect.

Methods

Methods, including statements of data availability and any associated accession codes and references, are available at https://doi.org/10.1038/s41567-017-0042-3.

Received: 25 May 2017; Accepted: 19 December 2017;
Published online: 12 February 2018

References

1. Schioppo, M. et al. Ultra-stable optical clock with two cold-atom ensembles. *Nat. Photon.* **11**, 48–52 (2017).
2. Al-Masoudi, A., Dörscher, S., Häfner, S., Sterr, U. & Lisdat, C. Noise and instability of an optical lattice clock. *Phys. Rev. A* **92**, 063814 (2015).
3. Nicholson, T. L. et al. Systematic evaluation of an atomic clock at 2×10^{-18} total uncertainty. *Nat. Commun.* **6**, 6896 (2015).
4. Ushijima, I., Takamoto, M., Das, M., Ohkubo, T. & Katori, H. Cryogenic optical lattice clocks. *Nat. Photon.* **9**, 185–189 (2015).
5. Huntemann, N., Sanner, C., Lipphardt, B., Tamm, C. & Peik, E. Single-ion atomic clock with 3×10^{-18} systematic uncertainty. *Phys. Rev. Lett.* **116**, 063001 (2016).
6. Chou, C. W., Hume, D. B., Koelemeij, J. C. J., Wineland, D. J. & Rosenband, T. Frequency comparison of two high-accuracy Al^+ optical clocks. *Phys. Rev. Lett.* **104**, 070802 (2010).
7. Huntemann, N. et al. Improved limit on a temporal variation of m_p/m_e from comparisons of Yb^+ and Cs atomic clocks. *Phys. Rev. Lett.* **113**, 210802 (2014).
8. Godun, R. M. et al. Frequency ratio of two optical clock transitions in $^{171}Yb^+$ and constraints on the time-variation of fundamental constants. *Phys. Rev. Lett.* **113**, 210801 (2014).
9. Riehle, F. Towards a redefinition of the second based on optical atomic clocks. *C. R. Phys.* **16**, 506–515 (2015).
10. Margolis, H. Timekeepers of the future. *Nat. Phys.* **10**, 82–83 (2014).
11. Vermeer, M. Chronometric levelling. *Rep. Finn. Geod. Inst.* **83**, 2 (1983).
12. Koller, S. B. et al. Transportable optical lattice clock with 7×10^{-17} uncertainty. *Phys. Rev. Lett.* **118**, 073601 (2017).
13. Cao, J. et al. A transportable $^{40}Ca^+$ single-ion clock with 7.7×10^{-17} systematic uncertainty. *Appl. Phys. B* **123**, 112 (2017).
14. Bongs, K. et al. Development of a strontium optical lattice clock for the SOC mission on the ISS. *C. R. Phys.* **16**, 553–564 (2015).
15. Pizzocaro, M. et al. Absolute frequency measurement of the $^1S_0$–$^3P_0$ transition of ^{171}Yb. *Metrologia* **54**, 102–112 (2017).
16. Denker, H. in *Sciences of Geodesy – II* (ed. Xu, G.) Ch. 5 (Springer, 2013).
17. Lisdat, C. et al. A clock network for geodesy and fundamental science. *Nat. Commun.* **7**, 12443 (2016).
18. Calonico, D. et al. High-accuracy coherent optical frequency transfer over a doubled 642-km fiber link. *Appl. Phys. B* **117**, 979–986 (2014).
19. Takano, T. et al. Geopotential measurements with synchronously linked optical lattice clocks. *Nat. Photon.* **10**, 662–666 (2016).
20. Barwood, G. P. et al. Agreement between two $^{88}Sr^+$ optical clocks to 4 parts in 10^{17}. *Phys. Rev. A* **89**, 050501 (2014).
21. Vogt, S. et al. A transportable optical lattice clock. *J. Phys. Conf. Ser.* **723**, 012020 (2016).
22. Leibrandt, D. R., Bergquist, J. C. & Rosenband, T. Cavity-stabilized laser with acceleration sensitivity below 10^{-12} g^{-1}. *Phys. Rev. A* **87**, 023829 (2013).
23. Levi, F. et al. Accuracy evaluation of ITCsF2: a nitrogen cooled caesium fountain. *Metrologia* **51**, 270 (2014).
24. Grebing, C. et al. Realization of a timescale with an accurate optical lattice clock. *Optica* **3**, 563–569 (2016).
25. Margolis, H. S. & Gill, P. Least-squares analysis of clock frequency comparison data to deduce optimized frequency and frequency ratio values. *Metrologia* **52**, 628–634 (2015).
26. *Report of the 104th Meeting of the Comité International des Poids et Mesures (CIPM)* (BIPM, 2015).
27. Nemitz, N. et al. Frequency ratio of Yb and Sr clocks with 5×10^{-17} uncertainty at 150 s averaging time. *Nat. Photon-.* **10**, 258–261 (2016).
28. Takamoto, M. et al. Frequency ratios of Sr, Yb, and Hg based optical lattice clocks and their applications. *C. R. Phys.* **16**, 489–498 (2015).
29. Akamatsu, D. et al. Frequency ratio measurement of ^{171}Yb and ^{87}Sr optical lattice clocks. *Opt. Express* **22**, 7898–7905 (2014); erratum **22**, 32199–32199 (2014).
30. Grosche, G. Eavesdropping time and frequency: phase noise cancellation along a time-varying path, such as an optical fiber. *Opt. Lett.* **39**, 2545–2548 (2014).

Acknowledgements

We would like to thank T. Zampieri for his technical support at LSM and A. Mura and Consorzio TOP-IX for technical help in the access to the optical fibre. The authors acknowledge funding from European Metrology Research Program (EMRP) Project SIB55 ITOC, the EU Innovative Training Network (ITN) Future Atomic Clock Technology (FACT), the DFG funded CRC 1128 geo-Q (Projects A03 and C04) and RTG 1728 and the UK National Measurement System Quantum, Electromagnetics and Time Programme. The EMRP is jointly funded by the EMRP participating countries within EURAMET and the European Union.

Author contributions

D.C. coordinated the measurement campaign with contributions from C.L., H.S.M. and Mi.Z.; J.G., S.K., S.V., S.H., U.S. and C.L. designed, built and operated the transportable Sr lattice clock; H.D., C.V. and L.T. made the geodetic measurements and calculated the local gravity potential values; A.R., F.N.B. and H.S.M. prepared, characterized and operated the transportable frequency comb; M.P., P.T., B.R., F.B., and D.C. designed, built and operated the Yb lattice clock; G.A.C. and F.L. designed, built and operated the INRIM Cs fountain, C.C. and A.T. designed, characterized and operated the optical fibre link between INRIM and LSM; C.C., P.B. and Ma.Z. operated the frequency comb at INRIM. J.G., C.C., M.P.,

© 2018 Macmillan Publishers Limited, part of Springer Nature. All rights reserved.

F.L., A.R., F.N.B., H.S.M., S.K. and C.L. contributed to the data analysis for the ratio and absolute frequency measurement. C.L. wrote the paper with support from H.S.M. and D.C. All authors discussed the results and commented on the paper.

Competing interests
The authors declare no competing financial interests.

Additional information
Reprints and permissions information is available at www.nature.com/reprints.

Correspondence and requests for materials should be addressed to C.L.

Publisher's note: Springer Nature remains neutral with regard to jurisdictional claims in published maps and institutional affiliations.

© 2018 Macmillan Publishers Limited, part of Springer Nature. All rights reserved.

Methods

Operation of lattice clocks. The realization and operation of the ^{171}Yb ($I=1/2$) and ^{87}Sr ($I=9/2$) clocks are very similar and have been presented in detail[12,15,21]. Ytterbium and strontium atoms are cooled to microkelvin temperatures in two-stage MOTs, exploiting the strong $^1S_0$–$^1P_1$ and weaker $^1S_0$–$^3P_1$ transitions (at 399 nm and 556 nm for Yb and 461 nm and 689 nm for Sr, respectively). The atoms are then trapped in one-dimensional optical lattices operating at the magic wavelengths[31] $\lambda^{Yb}_{magic}\approx 759$ nm and $\lambda^{Sr}_{magic}\approx 813$ nm, which to first order give a zero differential light shift between the $^1S_0$ and $^3P_0$ states.

Finally, the atoms are prepared for spectroscopy in a single magnetic sublevel m_f by optical pumping. As a result, shifts due to cold collisions and line pulling are reduced. The two π transitions from the $m_f=\pm 1/2$ sublevels in Yb ($m_f=\pm 9/2$ in Sr) are probed alternately at approximately halfwidth detunings so that the interrogation laser is locked to their average transition frequency. This effectively removes the linear Zeeman shift.

Uncertainties of lattice clocks. Here, we discuss the most important uncertainty contributions listed in Table 1. More details of the methods used to evaluate these uncertainties are given in refs [15,24] and [12].

Lattice light shifts. The lattice of the Yb clock is operated at $\nu_l=394{,}798.238$ GHz with a trap depth $U_0=196(4)E_r$ (E_r being the lattice recoil energy) and an atomic temperature of 7(3) μK as determined by sideband spectroscopy[32]. We measured the linear shift near the magic wavelength while the non-linear induced lattice light shift can be calculated using data from ref. [27].

For the Sr lattice clock, the typical lattice depth was about $100E_r$ as measured from sideband spectra[32]. These also yielded an atomic temperature of about 3.5 μK. The light-shift cancellation frequency was determined earlier; a reference resonator served as a wavelength reference during the experiments discussed here. The uncertainty of the linear lattice light shift allows for a possible resonator frequency change of 50 MHz caused by vibrations and shocks during transport and changes due to potential variations of the scalar and tensor light shift caused by geometrical changes or changes of the environmental magnetic field[33]. Without transport, the resonator frequency stays stable within 1 MHz for weeks, but relaxation during transport cannot be excluded. In future measurement campaigns, a determination of the light-shift cancellation wavelength will be made at the site of measurement. Higher-order light shifts were calculated using the coefficients in the same reference. As a check, three of the measurements in Fig. 2 were performed with a deeper lattice of about $160E_r$, which resulted in uncertainties for the linear lattice light shift and higher-order shifts of 29×10^{-17} and 1×10^{-17}, respectively. No significant variation of the measured frequency ratio R was observed.

Density shift. The density shift was evaluated in both lattice clocks by varying the interrogated atom number. Corrections for changes of the atomic temperature have been applied for the Sr clock. The lower uncertainty of the density shift at LSM is due to the lower atom number and thus density with which the clock was operated there.

BBR shift. The influence of BBR on the clock frequency has been discussed elsewhere[3,4,34–36]. Temperatures of the atomic environment were measured with calibrated platinum resistance thermometers. The uncertainty of the BBR shift is mostly related to temperature inhomogeneity. The representative temperature and its uncertainty are derived from the extreme temperatures found on the apparatus (the atomic oven is treated separately[12,15]) following the procedure described in ref. [37] for a rectangular probability distribution. The difference between the BBR corrections at LSM and INRIM is caused by different temperatures inside the trailer, as this temperature depends slightly on the outside temperature.

Other uncertainties. The uncertainties of servo error, second-order Zeeman shift and line pulling are reduced at INRIM by adjustments of experimental parameters, which were possible due to the more reliable operation.

H-maser as flywheel. A flywheel oscillator with good stability and high reliability, such as an H-maser, can be used to extend the averaging time between a less reliable system such as our Sr lattice clock and a Cs primary clock with lower stability[24]. The frequency ratio ν_{Sr}/ν_{Cs} was thus determined from the frequency ratios ν_{Sr}/ν_H and ν_H/ν_{Cs} using datasets with different lengths. The noise of the flywheel results in different average frequencies for these two intervals, but the additional uncertainty can be calculated[24] if the noise is well characterized, as it often is for masers. The calculation relies on Parseval's theorem, and uses the noise spectrum of the maser together with the Fourier transform of a weighting function that represents the two averaging intervals. For the full measurement-related uncertainty, this extrapolation uncertainty is combined with the statistical uncertainties of the maser calibration by the optical clock and the maser–Cs clock ratio over the extended interval. We modelled the maser noise by a superposition of flicker phase noise $6\times10^{-14}\,\tau^{-1}$ ($1\times10^{-13}\,\tau^{-1}$), white frequency noise $5\times10^{-14}\,\tau^{-1/2}$ ($4.5\times10^{-14}\,\tau^{-1/2}$) and a flicker noise 1.7×10^{-15} (1×10^{-15}) in March (May) 2016, respectively.

Gravity potential determination. To provide an accurate reference for the chronometric levelling, a state-of-the-art determination of the gravity (gravitational plus centrifugal) potential was performed, targeting the best possible uncertainty for each clock site. Spatial variations of the gravity potential are most important; corresponding temporal variations (mainly due to solid Earth and ocean tides) are below 0.07 $m^2\,s^{-2}$ for the potential difference between INRIM and LSM[38].

The static (spatially varying) gravity potential or corresponding potential differences can be determined by two classical geodetic methods[39]. The first is geometric levelling (together with gravity observations along the levelling path). The second (the so-called GNSS/geoid approach) uses GNSS positions (ellipsoidal heights) and the results from gravity field modelling, that is, a high-resolution (quasi)geoid model based on terrestrial and satellite gravity data. Both methods can be formulated in terms of either potential or height quantities. In the following discussion, metric units based on heights are generally preferred for simplicity, but corresponding potential values can easily be obtained by multiplying the height values by an average gravity value (e.g. 9.81 $m\,s^{-2}$). Geometric levelling is accurate at the millimetre level over short distances[40], but as a differential technique it can deliver only potential differences and is susceptible to systematic errors, which may accumulate to the few-decimetre level over continental distances. On the other hand, the GNSS/geoid approach can deliver absolute potential values; in this case the uncertainty depends mainly on the quality of the regional (quasi)geoid models, but the uncertainty of the GNSS positions also has to be considered.

New gravity measurements were made around the clock sites at INRIM and LSM to improve the reliability and uncertainty of the geopotential field modelling. These measurements included spot checks of the largely historic gravity database (consistency check), and the addition of new observations in areas so far void of gravity data (coverage improvement). Separate gravity surveys were carried out around INRIM and LSM, resulting in 36 and 123 new gravity points, respectively. The gravity surveys included one absolute gravity observation at INRIM and another at LSM, while the remaining points were observed with relative gravity meters (relative to the established absolute points), with 11 gravity points being located inside the Fréjus tunnel. Maps giving an overview of the distribution of gravity observations are given on the ITOC project page[41]. These new gravity observations as well as some other gravity updates (e.g. for Germany) were integrated into the terrestrial gravity database, the starting point being the version used to compute the previous European Gravimetric (Quasi)Geoid, EGG2008[16]. A consistency check between the new and existing gravity measurements showed no significant differences between the two data sets, confirming the quality of the entire database. However, a re-evaluation of the combined data-set revealed some old stations with obviously wrong positions, mainly located in France; these stations lie offroad and show large discrepancies between station and digital elevation model heights, and were therefore excluded from the (quasi)geoid computation.

A new (quasi)geoid model, EGG2015, was computed in a similar way to the previous EGG2008 model, using the remove–compute–restore procedure and the spectral combination approach, combining a global long-wavelength satellite gravity model with high-resolution terrestrial gravity and terrain data[16]. In addition to the new gravity measurements, enhancements included the use of a fifth-generation GOCE global geopotential model (GOCO05S)[42] and a spectral weighting scheme adapted to the GOCE model. The largest difference between the EGG2015 and EGG2008 input gravity values is about $3.5\times10^{-4}\,m\,s^{-2}$; for the output (quasi)geoid grids the largest difference is about 0.15 m. By far the largest differences are around the LSM site; they result from the new observations in areas previously void of gravity data and from the removal of gross errors related to some points in France with incorrect positions[16]. However, the maximum (quasi)geoid change at the two clock sites was less than 0.03 m. The uncertainty of EGG2015 was estimated in the same way as for EGG2008, resulting in a standard deviation of 2 cm, which holds for areas with a good coverage and quality of the terrestrial gravity field data, such as around INRIM (best-case scenario). However, around LSM the remaining data gaps in inaccessible areas and the strong spatial gravity field variation caused by the high mountains lead to a higher uncertainty estimate of about 4 cm.

The final relativistic redshift correction for the INRIM/LSM clock comparison was derived by the GNSS/geoid approach, although geometric levelling and gravity measurements were used to transfer the gravity potential from the nearest GNSS stations to the reference markers adjacent to the clocks at INRIM and LSM. The GNSS/geoid approach was chosen because the levelling data for Italy are rather old and do not include gravity corrections[43], and because the GNSS/geoid approach is not affected by systematic levelling errors. This resulted in a gravity potential difference of 10,029.7(6) $m^2\,s^{-2}$ between the two reference markers, and 10,032.1(16)$m^2\,s^{-2}$ between the actual clock positions at LSM and INRIM, respectively. The final uncertainty of the gravity potential difference between the reference markers nearest to the two clock positions (about 6 cm in terms of height) includes contributions from the (quasi)geoid in the Alpine region (approximately 5 cm, neglecting correlations[16]), the GNSS positions (1–2 cm) and the levelling connections (<1 cm, mainly from the tunnel portal to LSM). The larger uncertainty for the actual clock positions is because, for convenience and in view of the uncertainty of the chronometric levelling experiment, the height differences between the clock locations and the corresponding reference markers (less than 10 m apart) were determined using a simple spirit level rather than by geodetic levelling.

© 2018 Macmillan Publishers Limited, part of Springer Nature. All rights reserved.

INRIM–LSM frequency transfer. The remote clock comparison was performed by comparing the frequency of a link laser at 1,542.14 nm, sent from INRIM to LSM by a telecom optical fibre, with the frequencies of the clocks operated in the two locations. Two fibre frequency combs spanned the spectral gaps between the link laser and the clock interrogation lasers. The combs employed the transfer oscillator principle[44], making the measurements of the optical frequency ratios immune to the frequency noise of the combs. The frequency of the link laser was stabilized using a high-finesse cavity, whose long-term drift is removed by a loose phase-lock to a H-maser via a fibre frequency comb. As a result, the beat notes with the combs remained within a small frequency interval, facilitating long-term operation and reducing potential errors arising from any counter de-synchronization between INRIM and LSM[17].

The link laser used a multiplexed channel in the telecom fibre. Its path was equipped with two dedicated bidirectional erbium-doped fibre amplifiers that allowed a phase stable signal to be generated at LSM through the Doppler noise cancellation technique[17,18]. The contribution of fibre frequency transfer to the total fractional uncertainty was assessed to be 3×10^{-19} by looping back the signal from LSM using a parallel fibre. The occasional occurrence of cycle slips was detected by redundant counting of the beat note at INRIM. At LSM, the signal was regenerated by a diode laser phase locked to the incoming radiation with a signal-to-noise ratio greater than 30 dB at 100 kHz bandwidth; this ensured robust and cycle-slip-free operation.

In addition to the optical reference, a high-quality radiofrequency signal was needed at LSM to operate the Sr clock apparatus (frequency shifters and counters) and the frequency comb. Given the impossibility of having a GNSS-disseminated signal in the underground laboratory, a 100 MHz radiofrequency signal was delivered there by amplitude modulation of a second 1.5 μm laser that was transmitted through an optical fibre parallel to the first. At LSM, the amplitude modulation was detected on a fast photodiode, amplified and regenerated by an oven-controlled quartz oscillator at 10 MHz to improve the signal-to-noise ratio. The inherent stability of the free-running fibre link is in this case enough to deliver the radiofrequency signal with a long-term instability and uncertainty smaller than 10^{-13}. This resulting uncertainty contribution to the optical frequency ratio measurement is below 1×10^{-19}.

Averaging of the optical frequency ratio data. We made eight different optical frequency ratio measurements with a total measurement time of 15 h over a period of one week in May 2016 (Fig. 3). The data acquired on different days have different statistical and systematic uncertainties. We applied a statistical analysis that considers the correlations between the measurements from the different systematic shifts where the covariance matrix of the eight daily measurements is used to calculate a generalized least squares fit for the average[25,45]. We regarded the systematic uncertainties of the clocks (Table 1) as fully correlated, while the statistics related to the measurement duration were uncorrelated.

Absolute frequency of the Sr lattice clock. The chronometric levelling can be viewed from an alternative perspective: If we assume that the conventional measurement of the gravity potential difference is correct then we can deduce an average absolute frequency value of 429,228,004,229,873.13(40) Hz for the Sr lattice clock. The accuracy of the absolute frequency measurement achieved with the transportable clock is comparable to several recent measurements with laboratory systems[24,46–61].

Averaging the previously published values gives a frequency of 429,228,004,229,873.05(05) Hz. Together with the average Yb clock transition frequency of 518,295,836,590,863.75(25) Hz derived from other references[15,62–66], a Yb/Sr frequency ratio of 1.207,507,039,343,337,97(61) can be calculated (Fig. 3). This averaging assumes that there are no correlations between the different measurements.

Data availability. The data that support the plots within this paper and other findings of this study are available from the corresponding author upon reasonable request.

References

31. Katori, H., Takamoto, M., Pal'chikov, V. G. & Ovsiannikov, V. D. Ultrastable optical clock with neutral atoms in an engineered light shift trap. *Phys. Rev. Lett.* **91**, 173005 (2003).
32. Blatt, S. et al. Rabi spectroscopy and excitation inhomogeneity in a one-dimensional optical lattice clock. *Phys. Rev. A* **80**, 052703 (2009).
33. Westergaard, P. G. et al. Lattice-induced frequency shifts in Sr optical lattice clocks at the 10^{-17} level. *Phys. Rev. Lett.* **106**, 210801 (2011).
34. Middelmann, T., Falke, S., Lisdat, C. & Sterr, U. High accuracy correction of blackbody radiation shift in an optical lattice clock. *Phys. Rev. Lett.* **109**, 263004 (2012).
35. Safronova, M. S., Porsev, S. G., Safronova, S. U., Kozlov, M. G. & Clark, C. W. Blackbody radiation shift in the Sr optical atomic clock. *Phys. Rev. A* **87**, 012509 (2013).
36. Sherman, J. A. et al. High accuracy measure of atomic polarizability in an optical lattice clock. *Phys. Rev. Lett.* **108**, 153002 (2012).
37. JCGM (BIPM, IEC, IFCC, ILAC, ISO, IUPAC, IUPAP and OIML) *Evaluation of Measurement Data—Guide to the Expression of Uncertainty in Measurement* Vol. 100 (International Organization for Standardization, 2008); http://www.bipm.org/utils/common/documents/jcgm/JCGM_100_2008_E.pdf
38. Voigt, C., Denker, H. & Timmen, L. Time-variable gravity potential components for optical clock comparisons and the definition of international time scales. *Metrologia* **53**, 1365–1383 (2016).
39. Denker, H. et al. Geodetic methods to determine the relativistic redshift at the level of 10^{-18} in the context of international timescales—a review and practical results. *J. Geod.* https://doi.org/10.1007/s00190-017-1075-1 (2017).
40. Torge, W. & Müller, J. *Geodesy* 4th edn (De Gruyter, 2012).
41. European Metrology Research Programme Project SIB-55 *International Timescales with Optical Clocks* (2016); http://projects.npl.co.uk/itoc/project-structure/reg/gravity-observations/
42. Mayer-Gürr, T. et al. The combined satellite gravity field model GOCO05s. *Geophys. Res. Abstracts* **17**, EGU2015–12364 (2015).
43. Barzaghi, R. et al. Orthometric correction and normal heights for Italian levelling network: a case study. *Appl. Geomat.* **6**, 17–25 (2014).
44. Stenger, J., Schnatz, H., Tamm, C. & Telle, H. R. Ultra-precise measurement of optical frequency ratios. *Phys. Rev. Lett.* **88**, 073601 (2002).
45. Cox, M. G., Eiø, C., Mana, G. & Pennecchi, F. The generalized weighted mean of correlated quantities. *Metrologia* **43**, S268 (2006).
46. Boyd, M. M. et al. ^{87}Sr lattice clock with inaccuracy below 10^{-15}. *Phys. Rev. Lett.* **98**, 083002 (2007).
47. Baillard, X. et al. An optical lattice clock with spin-polarized ^{87}Sr atoms. *Eur. Phys. J. D.* **48**, 11–17 (2008).
48. Campbell, G. K. et al. The absolute frequency of the ^{87}Sr optical clock transition. *Metrologia* **45**, 539–548 (2008).
49. Hong, F.-L. et al. Measuring the frequency of a Sr optical lattice clock using a 120 km coherent optical transfer. *Opt. Lett.* **34**, 692–694 (2009).
50. Falke, S. et al. The ^{87}Sr optical frequency standard at PTB. *Metrologia* **48**, 399–407 (2011).
51. Yamaguchi, A. et al. Stability transfer between two clock lasers operating at different wavelengths for absolute frequency measurement of clock transition in ^{87}Sr. *Appl. Phys. Express* **5**, 022701 (2012).
52. Matsubara, K. et al. Direct comparison of a Ca^+ single-ion clock against a Sr lattice clock to verify the absolute frequency measurement. *Opt. Express* **20**, 22034–22041 (2012).
53. Le Targat, R. et al. Experimental realization of an optical second with strontium lattice clocks. *Nat. Commun.* **4**, 2109 (2013).
54. Falke, S. et al. A strontium lattice clock with 3×10^{-17} inaccuracy and its frequency. *New J. Phys.* **16**, 073023 (2014).
55. Akamatsu, D. et al. Spectroscopy and frequency measurement of the ^{87}Sr clock transition by laser linewidth transfer using an optical frequency comb. *Appl. Phys. Express* **7**, 012401 (2014).
56. Hachisu, H. et al. Direct comparison of optical lattice clocks with an intercontinental baseline of 9000 km. *Opt. Lett.* **39**, 4072–4075 (2014).
57. Lin, Y.-G. et al. First evaluation and frequency measurement of the strontium optical lattice clock at NIM. *Chin. Phys. Lett.* **32**, 090601 (2015).
58. Tanabe, T. et al. Improved frequency measurement of the $^1S_0$–$^3P_0$ clock transition in ^{87}Sr using a Cs fountain clock as a transfer oscillator. *J. Phys. Soc. Jpn.* **84**, 115002 (2015).
59. Lodewyck, J. et al. Optical to microwave clock frequency ratios with a nearly continuous strontium optical lattice clock. *Metrologia* **53**, 1123 (2016).
60. Hachisu, H., Petit, G. & Ido, T. Absolute frequency measurement with uncertainty below 1×10^{-15} using International Atomic Time. *Appl. Phys. B* **123**, 34 (2017).
61. Hachisu, H., Petit, G., Nakagawa, F., Hanado, Y. & Ido, T. SI-traceable measurement of an optical frequency at the low 10^{-16} level without a local primary standard. *Opt. Express* **25**, 8511–8523 (2017).
62. Kohno, T. et al. One-dimensional optical lattice clock with a fermionic ^{171}Yb isotope. *Appl. Phys. Express* **2**, 072501 (2009).
63. Lemke, N. D. et al. Spin-1/2 optical lattice clock. *Phys. Rev. Lett.* **103**, 063001 (2009).
64. Yasuda, M. et al. Improved absolute frequency measurement of the ^{171}Yb optical lattice clock towards a candidate for the redefinition of the second. *Appl. Phys. Express* **5**, 102401 (2012).
65. Park, C. Y. et al. Absolute frequency measurement of $^1S_0$ ($F=1/2$) mm–$^3P_0$ ($F=1/2$) transition of ^{171}Yb atoms in a one-dimensional optical lattice at KRISS. *Metrologia* **50**, 119–128 (2013).
66. Kim, H. et al. Improved absolute frequency measurement of the ^{171}Yb optical lattice clock at KRISS relative to the SI second. *Jpn J. Appl. Phys.* **56**, 050302 (2017).

© 2018 Macmillan Publishers Limited, part of Springer Nature. All rights reserved.